Published in Journal of Micromechanics and Microengineering 15, issue 12, 2372-2378, 2005
which should be used for any reference to this work

Generic technological platform for microfabricating silicon nitride micro- and nanopipette arrays

O T Guenat[1], S Generelli, M Dadras, L Berdondini, N F de Rooij and M Koudelka-Hep

Institute of Microtechnology, University of Neuchâtel, Rue Jaquet-Droz 1, CH-2007 Neuchâtel, Switzerland
E-mail: olivier.guenat@unine.ch

Abstract
In this paper, the design and the characterization of batch fabricated Si_xN_y micropipette arrays with diameters ranging from 6 μm down to 250 nm are described. The process used to fabricate the micromachined pipettes includes a deep reactive ion etching step, followed by the deposition of two successive layers, a thermal oxide layer and a low stress, low pressure chemical vapor deposited silicon nitride layer, respectively. The diameter of the micropipettes could be modulated simply by choosing the thicknesses of the oxide sacrificial layer and of the nitride walls of the micropipettes. The reactive ion etching of the micropipette top layer in deep cavities and in confined and deconfined configurations is discussed. The mechanical resistance of the micropipette array was qualitatively tested and it was demonstrated that a force of 0.25 mN/micropipette could be applied without rupture of the micropipettes.

1. Introduction

In the past few years, an important research effort has been carried out to develop arrays of micropipettes. The common terminology found in the literature describing free standing capillaries either in-plane or out-of-plane includes micropipettes, hollow microneedles and microcapillaries. In this paper, we will use the term micropipettes, except when referring to work by others, who preferred to use a different terminology.

In 2000, McAllister *et al* [1] reviewed various microfabrication techniques used to create microneedles for gene and drug delivery. Among the works reviewed, several types of micropipette arrays were presented: (a) an array of silicon dioxide hollow microcapillaries, (b) arrays of larger in-plane microfabricated probes and (c) hollow silicon and metallic microneedles arrays. Further studies based on a variety of fabrication techniques reported the development of silicon [2–5], silicon dioxide [6–8], silicon nitride [9, 10] and metallic in-plane [11] and out-of-plane [12] micropipette arrays, often with more complex designs and having solid and hollow bores with tapered and beveled tips.

The diameters of the micropipettes feature sizes from ten to hundreds of microns, except the SiO_2 hollow microcapillaries [13] quoted earlier, the Si_xN_y micropipettes fabricated in our group [9, 10] and the SiO_2 hollow microneedles presented in [8]. The micropipettes reported in these latter studies had diameters around 5 μm. Sub-micrometer silicon oxide nanopipette arrays with diameters of about 900 nm were reported in [14]. Using a rather complex process including a deep reactive ion etching (DRIE) to create hollow capillaries, a SF_6–Ar^+ plasma, for a progressive etching of the mask composed of silicon nitride and photoresist, the needle itself was realized by wet oxidation and a XeF_2 etching. The fabrication of even smaller micropipettes is possible using carbon nanotube technology. Carbon nanopipettes with a hollow core of a constant diameter of about 4–20 nm and lengths from a few microns to about 100 μm were achieved [15]. Unfortunately, this technology is not yet

[1] Present address: Center for Engineering in Medicine and Biology, Massachusetts General Hospital, Harvard Medical School, 51, Blossom Street, Boston, MA 02114, USA.

mature enough to batch fabricate nanopipettes with well-defined spatial positioning.

The increasing interest in micro- and nanopipette arrays and their potentially numerous applications ranging from cell transfection through drug delivery to nanosensors motivated our research for a more convenient (less complex), flexible technology platform allowing the modulation of the diameter and of the wall thickness of the micropipettes at will. To a certain extent the present development is based on nozzle technology [16] where a chemical vapor deposited (CVD) silicon oxide layer was used to decrease the nozzle aperture of a microfluidic injector. The deposition of this additional layer, however, resulted in an enlargement of the external diameter of the protruding nozzle. In order to avoid the enlargement of the external diameter, we present here a different approach based on the deposition of a silicon nitride layer in deep circular holes, which constitute the mold of the micropipette. The nitride layer deposited on top of a silicon dioxide sacrificial film allows the reduction of the internal micropipette diameter to a few hundred nanometers, as further described in this paper. Consequently, the micropipette wall thickness can accurately be defined simply by controlling the deposition rate of the silicon nitride layer. In our previous papers, we presented the development of arrays of 5 μm diameter and 50 μm high micropipettes with 500 nm thick walls made of low stress, low pressure chemical vapor deposited (LPCVD) silicon nitride [9, 10]. In this study, we present further developments of silicon nitride micropipettes with wall thicknesses ranging from 500 down to 50 nm. In addition, it must be emphasized that despite the reduction of the micropipette diameter, this technique preserves the length of the micropipettes, up to several tens of micrometers.

Another key point of the fabrication process was the opening of the top of the silicon nitride micropipettes. In contrast to Ryu *et al* [7], who opened their silicon dioxide micropipettes by mechanical polishing, enhancing the risk of clogging the micropipettes, and to [13], where the silicon dioxide microcapillaries were opened by wet etching (BHF), reactive ion etching (RIE) was chosen to remove the silicon nitride top. This was carried out by using the directional property of the reactive ion etching that permits us to preserve the micropipettes sidewalls. The openings of the top of the micropipettes in very deep and small cavities by using the same technique are also reported in this paper. Finally, the presentation of the fabrication limits of this generic technology and the mechanical robustness of the micropipettes are also discussed.

2. Design and micromachining process of the micropipettes

The micropipette arrays are fabricated using extensions and upgrades of previously reported design and microfabrication technologies [9, 10]. A double side polished, 390 μm thick, $\langle 1\,0\,0\rangle$ silicon wafer is coated with AZ1518 positive photoresist and patterned with arrays of 2 or 24 circular patterns of about 1.5–5 μm in diameter. The center-to-center spacing of these micropatterns varies from 100 to 750 μm. The patterned wafer is then etched by deep reactive ion etching (DRIE) forming cylindrical cavities with different etching

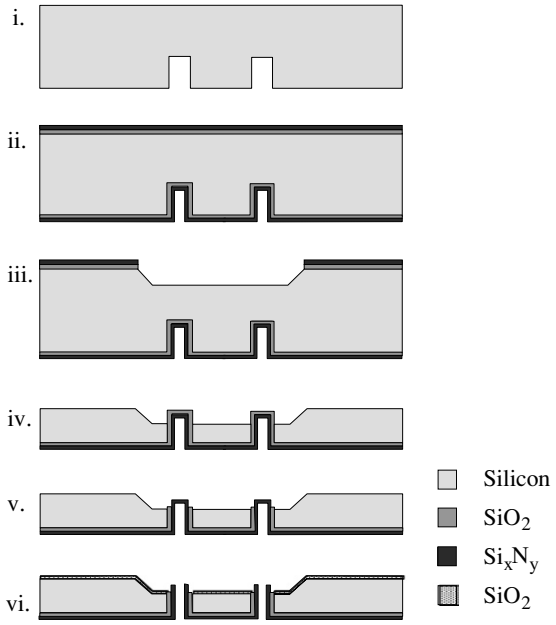

Figure 1. Cross-sectional flow layout of the major bulk-micromachining steps for the creation of the micropipette array.

depths (figure 1(i)). Depending on the aimed application of the micropipettes, their heights are selected between 15 and 50 μm. After DRIE and cleaning, a thermal wet dioxide layer that reduces the diameter of the cavities is grown on the silicon surface. Two thicknesses of the Si dioxide layer (1 μm and 1.4 μm) are investigated, in order to vary the final diameter of the micropipettes. A low stress Si_xN_y layer is then deposited by low pressure chemical vapor deposition (LPCVD) to form the walls of the micropipettes (ii). Low stress silicon nitride is preferred to standard LPCVD silicon nitride, since this non-stochiometric film that contains more silicon is nearly stress free [17]. This aspect is an important feature for the mechanical stability of the micropipettes. Different Si_xN_y thicknesses were investigated (from 100 nm up to 500 nm). The deposition of the low stress Si_xN_y is performed in three steps: first, a 15 nm thin stochiometric Si_3N_4 seed layer is deposited by using a gas ratio of NH_3 to dichlorosilane (DCS) of 3:1. Then, the ratio of ammonia to DCS is inversed to 1:5 for the deposition of the low stress silicon nitride layer. Finally, a 20 nm thin stochiometric Si_3N_4 layer is grown, as a protective and antioxidant layer. The deposition temperature is set around 800 °C.

Next, the silicon dioxide and nitride layers of the wafer top side are patterned simultaneously by RIE with large squares facing the cavities of the micropipettes and thinned down either by KOH etching (40%, 60 °C) (iii–iv) or by DRIE. These openings, which provide a protection for the micropipettes, are thinned down until the oxide tips of the latter are exposed. The oxide tips are wet etched in buffered HF (v), while the nitride caps of the tips are removed by RIE, using a SF_6 gas mixture. Finally, a 200 nm thin thermal oxide layer is grown onto the top side silicon surface as an electrical insulation (vi).

3. Experimental results

The two-layer technique allows the reduction of the external diameter of the micropipettes and the modulation

Table 1. Comparison of the tapered feature of the micropipettes at different phases of fabrication. Sets 1 and 2 summarize micropipette features with diameters of about 4 μm and 3 μm, respectively. The micropipettes described in this table had a 300 nm thick layer of low stressed LPCVD silicon nitride layer and had an overall length of 25 μm. The protruding length is indicated in the table. D_{bot} and D_{top} stand for the average diameter measured at the base and on the top of the protruding micropipettes, respectively. The angle α is the tapered angle of the micropipette, and n is the number of micropipettes measured with the SEM. The micropipette length indicated is the micropipette part protruding from silicon after KOH etching.

Set	Process	D_{bot} (μm)	D_{top} (μm)	n (–)	Micropipette length (μm)	Angle α (deg)
1	After DRIE	4.3	4.1	3	18.4	0.52
	Confined mode (RGV)	4.0	3.9	2	5.9	2.16
	Deconfined mode (RIE)	4.2	3.8	6	8.9	5.83
2	After DRIE	3.2	2.8	4	12.2	1.81
	Confined mode (RGV)	2.9	2.6	1	3.7	7.08
	Deconfined mode (RIE)	3.2	2.6	5	6.4	8.83

of the micropipettes wall thickness, while preserving the micropipette length and cylindricity obtained during the DRIE process. In other words, the micropipette length is only limited by the constraints of the DRIE process. In this study, the aspect ratio never exceeded 15:1, which is far under the DRIE limits. The cylindrical features of the DRIE opening can indirectly be observed by measuring the dimensions of a nitride micropipette that was previously molded in a deep circular hole etched in silicon (figure 2(*a*)). The tapered angle of the emerging micropipette is only of 0.5° over a length of 18 μm for a 4 μm micropipette. It is slightly larger for a 3 μm micropipettte (table 1). Figure 2(*b*) shows the cross-section of a micropipette with its wall made of 500 nm SiO_2 and 300 nm Si_xN_y.

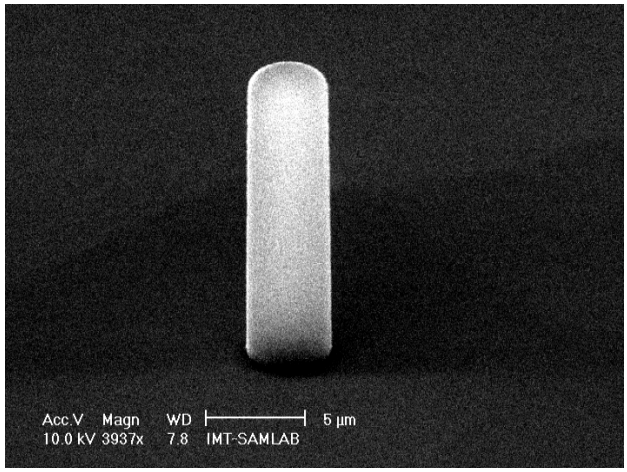

(*a*)

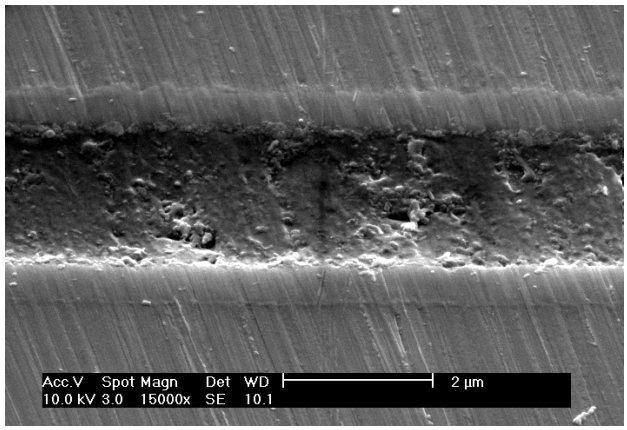

(*b*)

Figure 2. (*a*) SEM picture of the unopened micropipette after the KOH etching. (*b*) Cross-section of a micropipette prepared by diamond mechanical polishing, revealing the oxide and the nitride walls of the micropipette. The particles inside the micropipette are epoxy glue residues used to fill the micropipette prior to polishing.

3.1. Growth of thermal silicon oxide in deep circular holes

In contrast to planar geometry, where the formation of silicon dioxide (100% volume) occurs through the consumption of 44% of silicon (by volume), oxidation in circular holes leads to a drop in the oxidation rate. In this study, 15–20 μm deep hole arrays with diameters ranging from about 1.5 to 3.5 μm are etched by DRIE. Then, a thermal oxide layer is grown on the silicon. As a matter of fact, the stress associated with the non-uniform deformation of the oxide is responsible for the retardation of the oxide growth. The retardation is more severe at low temperatures on surfaces with small radii and on concave rather than convex surfaces [18–20]. In our experiment, the oxide thicknesses were estimated from SEM pictures for arrays of different diameters, on which a 1.4 μm nominal oxide layer was grown. Despite uncertainties introduced by the SEM measurements leading to the spreading of the data, the oxidation growth retardation is well illustrated in figure 3, and is observed for all the inspected wafers. For diameters larger than 4 μm, the oxide layer reaches about 80% of the nominal thickness, whereas it only attains about 30% of the nominal value for diameter smaller than 2 μm.

The dependence of the oxidation rate on the crystal orientation of the silicon surface is another phenomenon that can be observed when diameters are small. The orientation of the vertical surface of a cylindrical structure on a ⟨1 0 0⟩ silicon wafer varies periodically from ⟨1 0 0⟩ to ⟨1 1 0⟩ around the periphery. The ⟨1 1 0⟩ surface tends to oxidize faster than the ⟨1 0 0⟩ surface. Figure 4(*c*) depicts this phenomenon for a nanopipette with an external diameter of about 250 nm, resulting in the formation of a square-like silicon nitride micropipette. Furthermore, it should also be mentioned that the oxidation process in deep holes is obviously self-limiting, since when the oxide grown fills the trench, oxidation can no longer occur [20].

3.2. LPCVD low stress silicon nitride micropipettes

Once the oxide layer is grown in the holes, the silicon nitride layer can subsequently be deposited, to form the micropipettes

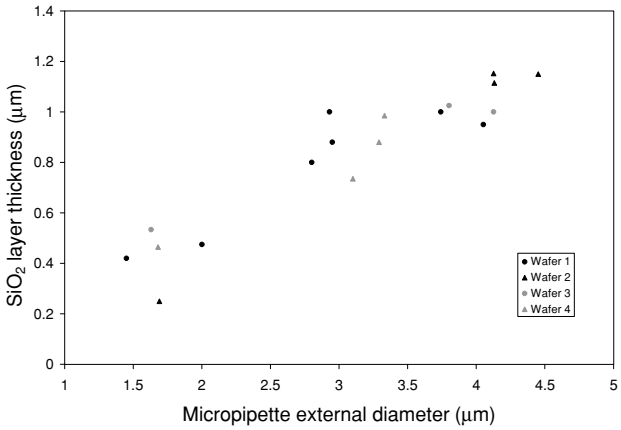

Figure 3. Oxide thickness versus external diameter of the micropipette. The results were obtained from four different wafers. The nominal thickness was 1.4 μm. The thicknesses were measured after the BHF etch of the micropipette top.

walls. LPCVD low stress silicon nitride was chosen since this non-stochiometric film has a number of features that are interesting for the micropipette applications. Besides its almost stress-free feature [17] and Young's modulus about half of that of stochiometric silicon nitride [21], making it less vulnerable to stress [22], it can also be deposited uniformly with regards to film thickness, composition and conformal step coverage [23].

Another important aspect, general to all silicon nitride films, is the possibility of etching them selectively by reactive ion etching techniques. Unlike wet etching, reactive ion etching is inherently very directional [24, 25] and thus preserves the sidewalls of the micropipettes. In this study, we used the Alcatel plasma etching system GIR 263 equipped with a confined (RGV) and deconfined system (RIE). The main differences between these two modes consist of different inter-electrode distances and in distinct plasma powers for each mode. The inter-electrode distance is set between 3 and 5 mm for the RGV mode with a plasma power of 230 W, whereas the RIE mode is operated at a lower plasma power (150 W) and a larger inter-electrode distance of 150 mm.

3.2.1. Modulation of the diameter and of the wall thickness of the micropipette. Low stress LPCVD silicon nitride layers

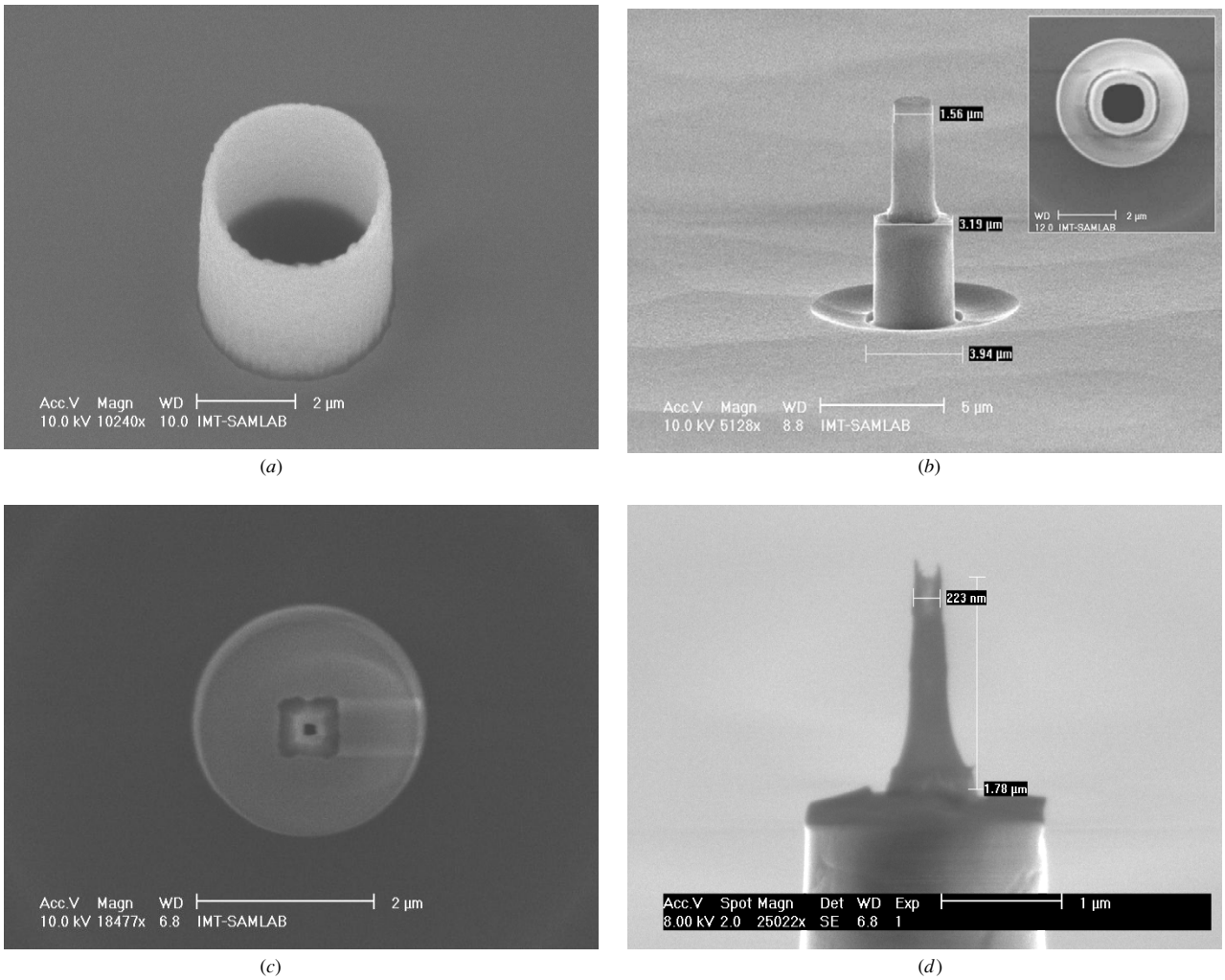

Figure 4. SEM pictures of micropipettes with different diameters: (*a*) diameter 3.5 μm with 150 nm nitride walls, (*b*) diameter 1.5 μm with 300 nm walls, (*c*, *d*) nanopipette with 220 nm diameter and 50 nm walls. The inner diameter of the nanopipette is estimated to be about 120 nm. The dependence of the oxide growth versus the crystal orientation can be seen in (*c*).

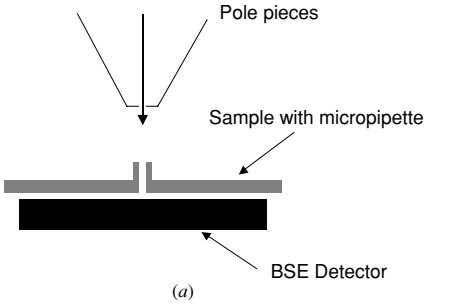

(*a*)

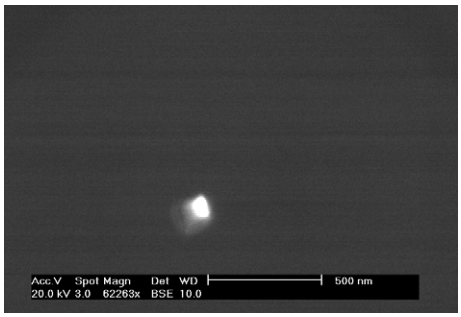

(*b*)

Figure 5. (*a*) Experimental set-up for the determination of the opening of the nanopipette. The latter is aligned in a SEM, between the pole piece and the back scattered electron (BSE) detector. (*b*) A 70 nm spot is observed on the BSE detector indicating that electrons passed through the nanopipette.

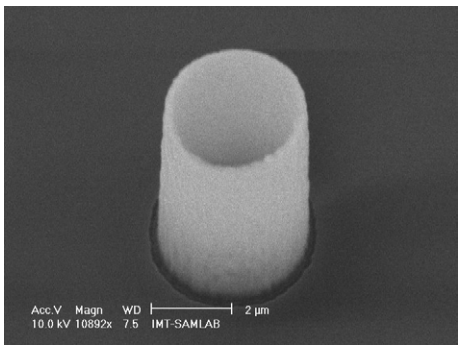

(*a*)

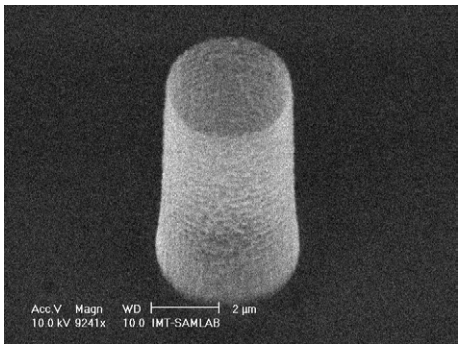

(*b*)

Figure 6. Etching difference between (*a*) confined (RGV) and (*b*) deconfined (RIE) modes for identical micropipettes (4 μm in diameter).

with thicknesses ranging from 100 to 500 nm were deposited either with or without a sacrificial SiO_2 layer. Figure 4(*a*) shows a SEM picture of a 3.5 μm micropipette (35 μm total length) with a silicon nitride wall of about 150 nm. Smaller micropipettes with an external diameter of about 1.6 μm were realized with a 0.55 μm thin oxide sacrificial layer (figure 4(*b*)). The bottle-like shape results from silicon oxide BHF etching followed by an additional KOH etching. The small annular recess at the bottom of the micropipette was observed only in the presence of an oxide layer. It might be due to the configuration of the plasma at the bottom of the micropipette, around the cavity created by the oxide under etch.

By further increasing the thickness of the sacrificial oxide layer, a micropipette with submicrometer size diameters could be realized. Figures 4(*c*) and 4(*d*) illustrate a 15 μm long (total length) nanopipette with an external diameter of about 250 nm. The internal diameter of the nanopipette was estimated from SEM and found to be in the order of 120 nm. A STEM (scanning transmission electronic microscopy) investigation was carried out to demonstrate that the nanopipette was effectively opened on the whole length. A backscattered electron (BSE) detector was installed below the sample as presented in figure 5(*a*). The electrons that pass through the opened nanopipette can be detected by the BSE detector. A small 70 nm spot (figure 5(*b*)) effectively confirmed that the nanopipette was completely opened. The non-uniform hollow around the spot might be related to the misalignment between the nanopipette and the detector.

3.2.2. Etching difference between confined and deconfined modes. It must be pointed out that during the reactive ion etching all the walls of the micropipettes were thinned down. This phenomenon can clearly be observed at the walls of the nanopipette where they are etched from 300 nm down to about 50 nm on the top of the nanopipette. The choice of the etching mode plays an important role in this respect. The deconfined mode (RIE) that was used to etch this nanopipette would create a significantly larger tapered angle than the confined mode (RGV). Table 1 summarizes the tapered angles obtained for micropipettes with similar diameters etched with both methods. The tapered angle more than doubled between the two modes for 4 μm diameter micropipettes. Figure 6 clearly reveals the shape difference of two identical micropipettes etched either with one or the other mode. For smaller micropipettes (3 μm), the tapered angle was larger for both modes, but the walls of the micropipettes opened with the deconfined mode were so thin that they were partially damaged. This effect can be explained by the nature of the etching configuration. The proximity of the electrodes in the RGV mode leads to a more directional ion bombardment than in the RIE configuration; therefore, the etching rate is also much higher for the confined mode. Considering the particular aspect of the design and the fact that the nitride layer is etched in a 360 μm deep KOH cavity, the etching rate obtained with the RGV configuration was found to be about four times larger (about 28 Å s^{-1}) than that obtained in the RIE mode.

3.2.3. Etching in deep and small grooves. All of the micropipettes presented above were located at the bottom of a 2 $\times$ 2 mm^2 KOH groove at a depth of 360 μm. The reproducibility of the micropipette shape was found to be

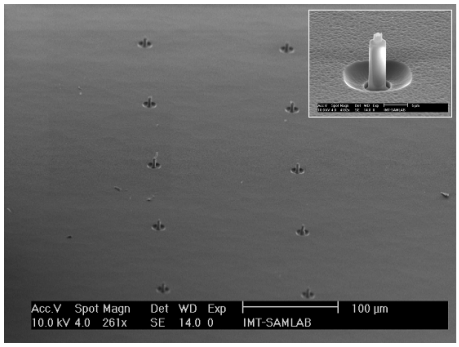

(*a*)

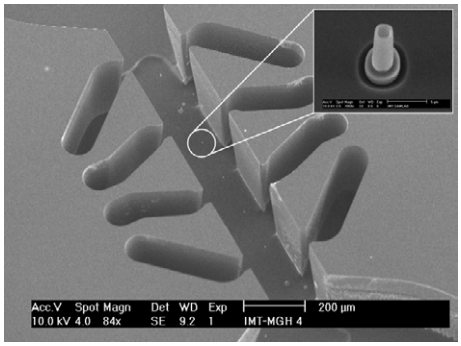

(*b*)

Figure 7. Micropipette arrays etched in (*a*) a deep KOH groove and (*b*) a deep DRIE microchannel.

excellent for the entire array, as well as at the wafer level. Figure 7(*a*) presents a SEM picture of a 1.7 μm micropipette array that was fabricated with a 2 μm thick oxide layer. In this example, the latter layer was partially etched after the reactive ion etching. Micropipette arrays could also be fabricated in much narrower and deep cavities as illustrated in figure 7(*b*) showing an array of 16 micropipettes at the bottom of a 200 μm wide and 365 μm deep microchannel [26].

3.3. Mechanical and piercing properties of the micropipette array

The mechanical stability of the micropipettes was qualitatively tested by pressing a 6.3 μm thin Al foil (Alcan Aluminium Valais SA, Sierre, Switzerland) on a micropipette array. This technique was already used by Griss *et al* [3] to demonstrate the robustness of larger microfabricated microneedles. As an example, an array of 20 μm long and 4 μm in diameter micropipettes was used for this test. After the micropipettes were inserted, the Al foil and the micropipettes were inspected by scanning electron microscopy. Figure 8(*b*) illustrates a micropipette emerging without any damage from the Al foil. During the operation, a portion of the latter remained on the top part of the micropipette. The Al foil was pressed with a small rubber probe (10×10 mm^2) against the micropipette array with an estimated force of 2 N (figure 8(*a*)). Thus, the force applied on one micropipette is in the order of 0.25 mN. This corresponds, for example, to more than six times the force required to puncture skin (pressure to puncture skin = 3.18 MPa [27]).

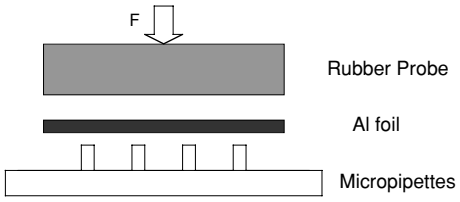

(*a*)

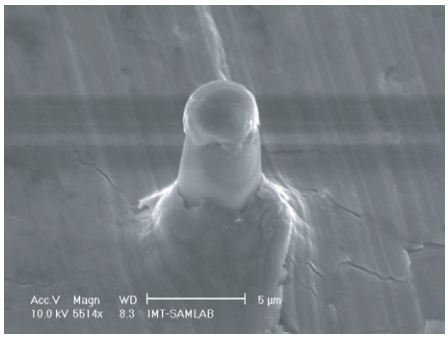

(*b*)

Figure 8. (*a*) Experimental set-up: an aluminum foil was pressed against the micropipette array with a rubber probe. (*b*) A micropipette emerging from a 6.3 μm thick Al foil without breaking. A residual Al film remained on the top of the micropipette.

4. Conclusion

The technology presented in this paper allowed the batch microfabrication of low stress silicon nitride micropipette arrays with diameters ranging from 6 μm down to 250 nm, with thicknesses of walls of 500 nm down to 50 nm. The flexibility of this generic technological platform is first based on a two-layer technique that allows the modulation of the diameter of the micropipettes by selecting the thicknesses of the oxide sacrificial layer and of the nitride walls of the micropipettes. Secondly, the thicknesses of the walls can exactly be defined by setting the thickness of the nitride layer and thus be controlled at some tens of nanometers. In addition, the thicknesses and the shapes of the walls on the top of the micropipette can be fine-tuned by choosing the plasma etching configuration. Thirdly, the apparent height of the micropipette can also be precisely defined by fine-tuning either the KOH or DRIE etchings of the silicon surrounding the micropipette array.

The excellent reproducibility of the micropipettes at the wafer level and the process simplicity make this generic technology an invaluable tool for numerous purposes, especially micro- and nanotools for biomedical applications.

Acknowledgments

The authors express their gratitude to the COMLAB team, in particular P-A Clerc, G Mondin and N Hegelbach for their valuable help. Special thanks goes to M Leboeuf for the preparation of the micropipette thin slice. Thanks also goes to Dr P Pouly and Dr A Howell for providing the 6.3 μm thin Al foil (Alcan Aluminium Valais SA, Sierre, Switzerland). SGe and OTG thank the Swiss National Science Foundation for respectively SNF project 2005321-103961 and the SNF advanced researcher grant PA00A-105032.

References

[1] McAllister D V, Allen M G and Prausnitz M R 2000 Microfabricated microneedles for gene and drug delivery *Annu. Rev. Biomed. Eng.* **2** 289–313

[2] Stoeber B and Liepmann D Two-dimensional arrays of out-of-plane needles *Proc. from the 2000 Int. Mechanical Engineering Congress and Exposition (Orlando, FL, November 2000)*

[3] Griss P and Stemme G 2002 Novel, side opened out-of-plane microneedle for microfluidic transdermal interfacing *Proc. MEMS* pp 467–70

[4] Gardeniers J, Berenschot J, de Boer M, Yershurun Y, Hefetz M, van't Oever R and v den Berg A Silicon micromachined hollow microneedles for transdermal liquid transfer *Proc. MEMS 2002 (Las Vegas, NV)* pp 141–4

[5] Mukerjee E, Issereoff R, Collins S and Smith R 2003 Microneedle array with integrated microchannels for transdermal sample extraction and *in-situ* analysis *Proc. Transducers (Boston, MA)* pp 1439–41

[6] Ohigashi R, Tsuchiya K, Mita Y and Fujita H 2001 Micro capillaries array head for direct drawing of fine patterns *Proc. MEMS (Interlaken, Switzerland)* pp 389–92

[7] Ryu K S, Fan Z and Liu C 2002 Microfabricated process for high-density micropipette array and matching multi-well plate with mixers *Proc. μTAS (Nara, Japan)*

[8] Valera E, Molinero D, Rodriguez A and Alcubilla R 2004 Fabrication of silicon oxide microneedles from macroporous silicon *Proc. Nanoelectronic and Photonic Systems Workshop, IEEE Tarragona* pp 65–6

[9] Guenat O, Wang X, Dufour J F, van der Wal P, Morf W E, de Rooij N and Koudelka-Hep M 2003 Ion-selective microelectrode array for intracellular detection on chip *Proc. Transducers, (Boston, MA)* pp 1063–6

[10] Guenat O, Dufour J F, van derWal P, Morf W, de Rooij N F and Koudelka-Hep M 2005 Microfabrication and characterization of an ion-selective microelectrode array platform *Sensors Actuators* B **105** 65–73 (special issue)

[11] Papauptsky I, Brazzle J, Swerdlow H, Weiss R and Frazier A B 2000 Micromachined pipette arrays *IEEE Trans. Biomed. Eng.* **47** 812–9

[12] Kim K, Park D S, Lu H M, Che W, Kim K, Lee J-B and Ahn C H 2004 A tapered hollow metallic microneedle array using backside exposure of SU8 *J. Micromech. Microeng.* **14** 597–603

[13] Chun K, Hashiguchi G, Toshiyoshi H and Fujita H 1999 Fabrication of hollow microcapillaries used for injection of genetic materials into animal/plant cells *Japan. J. Appl. Phys.* **38** 279–81

[14] Cabodevila G, Lepioufle B and Fujita H 2002 Arrayed micro needles for mechanical gene insertion *Proc. SPIE, Biomedical Applications of Micro- and Nanoengineering* **4937** 90–7

[15] Mani R C, Li X, Sunkara M K and Rajan K 2003 Carbon nanopipettes *Nano Lett.* **3** 671–3

[16] Luginbuhl P *et al* 2000 Femtoliter injector for DNA mass spectrometry *Sensors Actuators* B **63** 167–77

[17] van Zeijl H W, Mijacovic S and Nanver L K 2001 Electrical detection and simulation of stress in silicon nitride spacer technology *J. Mater. Sci., Mater. Electron.* **12** 339–41

[18] Kao D B, McVittie J P, Nix W D and Saraswat K C 1987 Two dimensional thermal oxidation of silicon—I. Experiments *lEEE Trans. Electron Devices* **34** 1008–17

[19] Kao D B, McVittie J P, Nix W D and Saraswat K C 1988 Two dimensional thermal oxidation of silicon—II. Modeling stress effects in wet oxides *IEEE Trans. Electron Devices* **35** 25

[20] Xu Y *et al* 2002 A physically-based model for oxidation in a circular trench in silicon *Proc. Nanotech 2002, ICCN-MSM 2002 (Puerto Rico)*

[21] Kiesewetter L, Zhang J M, Houdeau D and Steckenborn A 1992 Determination of Young's moduli of micromechanical thin films using resonance method *Sensors Actuators* A **35** 153–9

[22] Fan L S, Howe R T and Müller R S 1990 Fracture toughness characterization of brittle thin films *Sensors Actuators* **A21–A23** 872–4

[23] Gardeniers J G E, Tilmans H A C and Visser C C G 1996 LPCVD silicon rich nitride films for applications in micromechanics studied with statistical experimental design *J. Vac. Sci. Technol.* A **14** 2879–92

[24] Jansen H, Gardeniers H, de Boer M, Elwenspoek M and Fluitman J 1996 A survey on the reactive ion etching of silicon in microtechnology *J. Micromech. Microeng.* **6** 14–28

[25] Oehrlein G, Doemling M, Kastenmeier B, Matsuo P, Rueger N, Schaepkens M and Standaert T 1999 Surface science issues in plasma etching *IBM J. Res. Dev.* **43** 181

[26] Guenat O T, Generelli S, Clerc P-A, de Rooij N F, Koudelka-Hep M, Berthiaume F and Yarmush M L 2005 Development of a platform for microscale monitoring of cell function and differentiation *Proc. 3rd Annu. Int. IEEE-EMBS Special Topic Conf. on Microtechnologies in Medicine and Biology (Hawaii, May 2005)* p 77

[27] Aggarwal P and Johnson C R 2004 Geometrical effects in mechanical characterizing of microneedle for biomedical applications *Sensors Actuators* B **102** 226–34